noted that such a high diffusion of the canard vortex may cause significant problems for the numerical prediction of the load on the wing, particularly when simple potential methods, which do not consider any diffusion effects, are used.

Acknowledgments

References

[1]Buresti, G., and Lombardi, G., "Indagine sperimentale sull'interferenza ala-canard," (Experimental Analysis on Wing-Canard Interference), L'Aerotecnica, Missili e Spazio, Vol. 67, March–Dec. 1988, pp. 47–57.

[2]Lombardi, G., and Morelli, M., "Pressure Measurements on a Forward-Swept Wing-Canard Configuration," Journal of Aircraft, Vol. 31, No. 2, 1994, pp. 469–472.

[3]Buresti, G., Lombardi, G., and Polito, L., "Analysis of the Interaction Between Lifting Surfaces by Means of a Non-Linear Panel Method," Boundary Integral Method Theory and Applications, edited by L. Morino and R. Piva, Springer–Verlag, Berlin, 1991, pp. 125–134.

[4]Buresti, G., Lombardi, G., and Petagna, P., "Wing Pressure Loads in Canard Configurations: A Comparison Between Numerical Results and Experimental Data," Aeronautical Journal, Vol. 96, Aug.–Sept. 1992, pp. 271–279.

[5]Tu, E. L., "Vortex-Wing Interaction of a Close-Coupled Canard Configuration," Journal of Aircraft, Vol. 31, No. 2, 1994, pp. 314–321.

[6]Freestone, M. M., "Vorticity Measurement by a Pressure Probe," Aeronautical Journal, Vol. 92, Jan. 1988, pp. 29–35.

[7]Cordova, D., and Manacorda, G., "Tecniche di Misura della Vorticità nella Scia di Corpi," (Vorticity Measurement Techniques in Body Wakes), M.S. Thesis in Aeronautical Engineering, Dept. of Aerospace Engineering, Univ. of Pisa, Pisa, Italy, July 1992.

[8]Cannizzo, F., and Ricca, A., "Sviluppo ed Applicazioni di nuove Metodologie per la Caratterizzazione di Scie di Superfici Portanti," (Development and Applications of New Methods for the Characterization of Lifting Surface Wakes), M.S. Thesis in Aeronautical Engineering, Dept. of Aerospace Engineering, Univ. of Pisa, Pisa, Italy, July 1994.

[9]Takahashi, R. K., and McAlister, K. W., "Preliminary Study of a Wing-Tip Vortex Using Laser Velocimetry," NASA TM 88343, Jan. 1987.

Computational Study of a Conical Unit Aspect Ratio Wing at Supersonic Speeds

Brian E. McGrath*
Lockheed Engineering and Sciences Company, Inc., Hampton, Virginia 23666

Nomenclature

b = wingspan
C_D = drag coefficient, drag/$q_\infty S$

*Senior Engineer, Aeronautical Sciences Section. Senior Member AIAA.

C_L = lift coefficient, lift/$q_\infty S$
C_p = pressure coefficient, $p - p_\infty/q_\infty$
M = Mach number
M_N = component of the Mach number normal to the wing leading edge = $M_\infty \cos \Lambda \sqrt{1 + \sin^2\alpha \tan^2\Lambda}$
p = pressure
p_{t_2}/p_{t_∞} = total pressure ratio
q = dynamic pressure, $\frac{1}{2}\rho V^2$
S = wing reference area
V = velocity
y = spanwise coordinate
α = angle of attack
α_N = angle of attack normal to the wing leading edge = $\tan^{-1}(\tan \alpha/\cos \Lambda)$
$\alpha_{N_{corr}}$ = angle of attack normal to the wing leading edge corrected for thickness = $\alpha_N - \delta_f$
δ_f = streamwise leading-edge flow deflection angle
Λ = wing leading-edge sweep
ρ = density

Subscripts

t = total flow conditions (i.e., flow conditions if flow is brought to rest isentropically)
2 = flow conditions downstream of a shock wave or local flow conditions
∞ = freestream flow conditions

Introduction

F UTURE advanced high-performance military aircraft designs will be required to have high levels of aerodynamic performance and low radar cross section for survivability. These design requirements apply to various advanced military aircraft from missiles to bombers. A well-known common geometric characteristic of all highly survivable vehicles is sharp planform edges. The design requirement of a sharp-edge planform for increased survivability integrates well with the aerodynamic design philosophy for efficient supersonic flight. The focus of the present study is to assess the utility of a general computational method that may be applied to a variety of advanced military designs over a broad Mach number range.

A literature review of the current supersonic analysis and design methods identified an Euler equation code named the Euler Marching Technique for Accurate Computation (EMTAC[1,2]) as a promising preliminary computational analysis and design tool. The literature review also identified a candidate geometry for the assessment of EMTAC. The selected geometry is a conical delta wing of unit aspect ratio shown in Fig. 1. This geometry was chosen because the wing is conical and representative of the class of geometry of interest. Experimental results for this geometry have been documented extensively.[3,4]

This study compares results from computational analysis and experimental tests. The study results are presented for C_L, C_D (integrated from the surface C_p distribution), and the
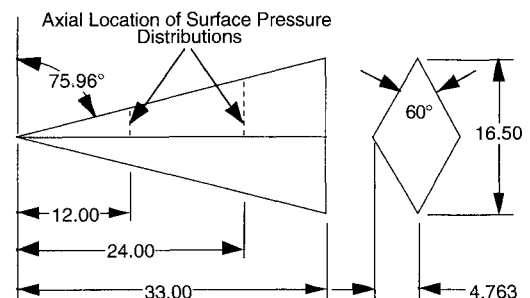

Fig. 1 Description of geometry showing x locations of the surface pressure distributions. (All dimensions are in inches.)

surface C_p distribution for Mach numbers 2.8 and 4.0. The estimation of C_D includes only the contribution of pressure and not skin friction. An assessment and comparison of the flowfield characteristics are presented using contour plots of several computational flowfield quantities and upper-surface flowfield classification studies on delta wings.[5-9]
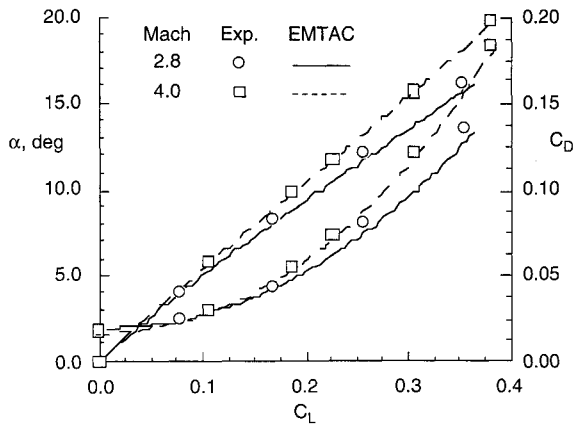

Fig. 2   Comparison of lift coefficient and inviscid drag coefficient between EMTAC and experiment at M_∞ = 2.8 and 4.0.
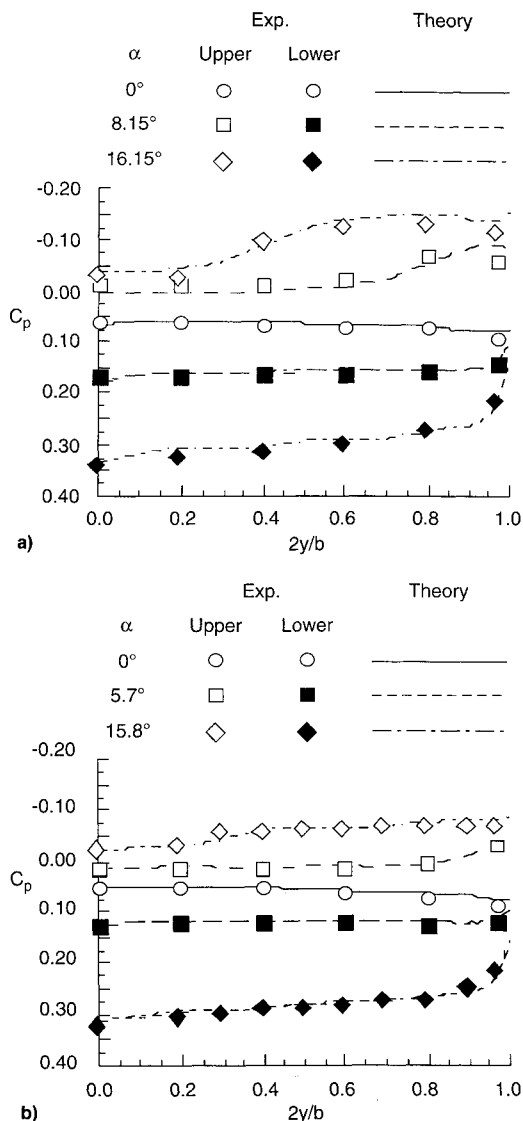

Fig. 3   Comparison of the surface pressure distributions between EMTAC and experiment: a) M_∞ = 2.8, x = 24 in. and b) M_∞ = 4.0, x = 24 in.

Discussion

Figure 2 shows C_L as a function of α and the inviscid drag polar. Comparison between EMTAC and experiment shows good agreement for C_L and the inviscid drag polar at each Mach number. Comparison of the zero-lift wave drag between EMTAC and experiment shows good agreement at each Mach number.

Comparison of the surface C_p distributions between EMTAC and experiment are presented in Fig. 3a (M_∞ = 2.8) and 3b (M_∞ = 4.0). The figure presents the C_p distribution at a single streamwise location (x = 24 in.) and three angles of attack. In general, Fig. 3 shows that EMTAC provides a good prediction of the C_p distribution along the upper and lower wing surfaces for all angles of attack and Mach numbers presented. Overall, EMTAC did not completely capture the exact levels or complete shape of the surface pressure distributions at each angle of attack and Mach number. However, EMTAC did capture the basic trends, overall levels, and gen-
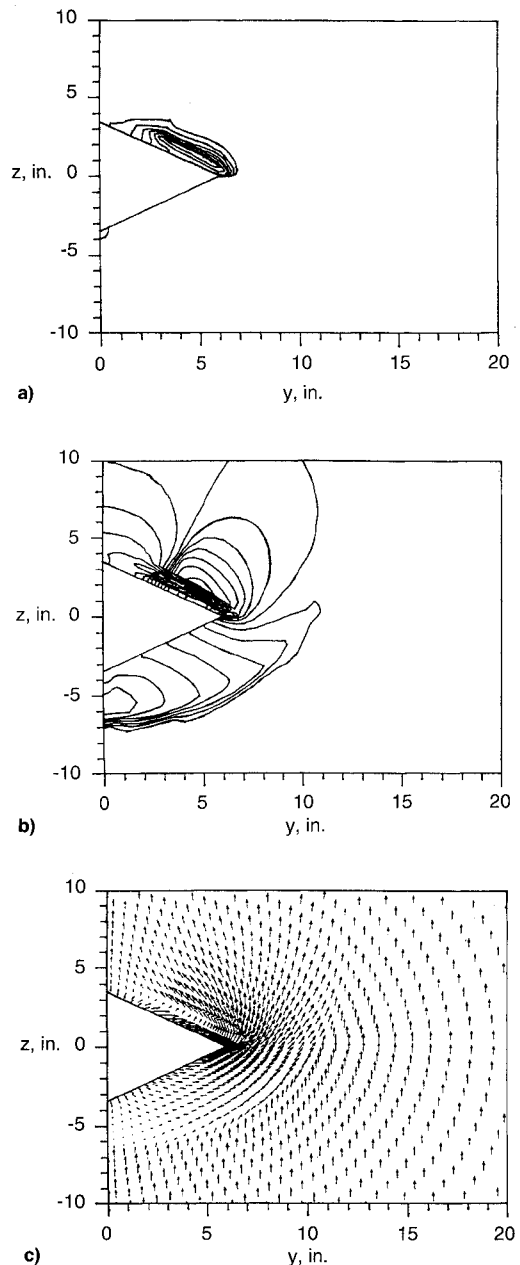

Fig. 4   Flowfield results from EMTAC at M_∞ = 2.8, α = 16.15 deg: a) total pressure ratio contours, b) crossflow Mach number contours, and c) crossflow velocity vectors.

eral shape of the surface pressure distributions, which provide a high level of confidence in the application of EMTAC for preliminary analysis of advanced vehicle configurations.

Flowfield properties obtained by EMTAC solutions are presented in Figs. 4 and 5 for $M_\infty = 2.8$, $\alpha = 16.15$ deg and $M_\infty = 4.0$, $\alpha = 15.8$ deg, respectively. The flowfield properties are presented as contour plots of the following properties: the total pressure ratio, crossflow Mach number, and crossflow velocity vectors. The individual contour levels are not specified on each figure. However, a qualitative assessment of the flowfield characteristics is given. The contour plots are used to show the existence or nonexistence of attached flow, rotational or vortex flow, and embedded crossflow shocks.

Figure 4 shows results at $M_\infty = 2.8$, $\alpha = 16.15$ deg. The concentrically-shaped total pressure contours along the upper surface indicate a total pressure loss usually associated with rotational or vortex flow. The swirling nature of the crossflow
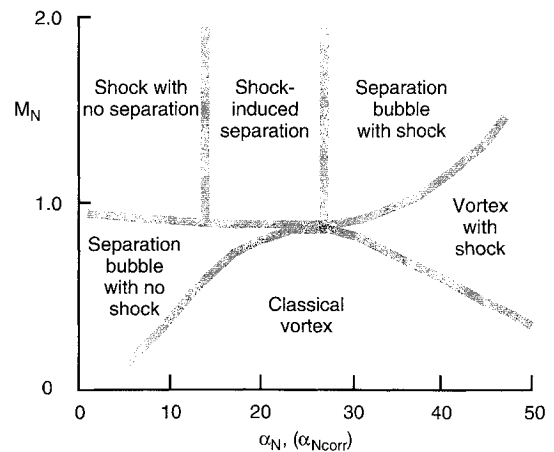
Fig. 6 Flow classification chart for delta wings.

velocity vectors also shows the region of rotational or vortex flow. Both the crossflow Mach number contours and the crossflow velocity vectors show the presence of a crossflow shock along the upper surface near the midspan. The coalescence of the crossflow Mach number contours along a line indicate the presence of a crossflow shock, and the crossflow shock is also observed in the crossflow velocity vectors by the abrupt decrease in velocity vector length along a line within the flowfield. These observations suggest that a vortex with a shock forms along the upper surface of the configuration.

Figure 5 shows results at $M_\infty = 4.0$, $\alpha = 15.8$ deg. The total pressure shows concentrically-shaped contours representing a total pressure loss along the upper surface that typically indicates rotational or vortex flow. The swirling nature of the crossflow velocity vectors also indicates rotational flow. The crossflow velocity vectors and the crossflow Mach number contours indicate the presence of a crossflow shock. These observations suggest the presence of a vortex with an embedded crossflow shock along the upper surface of the geometry.

A comparison of the flowfield characteristics described in Figs. 4 and 5 is made to upper-surface flow classification studies of flat delta wings. Figure 6 shows the representation of upper-surface flow classification of flat delta wings.[5-8] The data are correlated using two parameters, M_N and α_N. To compare the thick delta wing results to the flat delta wing results, corrections are made to α_N for thickness.[8] From the corrected flow classification parameters, the expected leeside flow type is determined from Fig. 6.

Using the upper-surface flow classification figure, the leeside flow at $M_\infty = 2.8$, $\alpha = 16.15$ deg ($M_N = 1.02$, $\alpha_{N_{corr}} = 41.8$ deg) is characteristic of a vortex with shock. The Euler code captures the crossflow shock and a region of rotational flow along the upper surface suggesting the presence of a vortex with shock. The leeside flow classification at $M_\infty = 4.0$, $\alpha = 15.8$ deg ($M_N = 1.43$, $\alpha_{N_{corr}} = 41.2$ deg) is a separation bubble with shock. The EMTAC results capture the crossflow shock and a region of rotational flow along the upper surface, possibly suggesting a vortex or region of circulation with a shock. The comparison of the upper-surface flow classification and EMTAC shows similarities with the empirically correlated and computed flowfield characteristics for most flow conditions.

Concluding Remarks

The objective of this study was to identify and assess a computational method as a preliminary analysis and design tool for advanced military aircraft designs. Computational results were compared with experiment for a thick unit aspect ratio delta wing at freestream Mach numbers of 2.8 and 4.0.

Results compared for the force coefficients show that EM-TAC accurately predicted the lift and inviscid drag over the
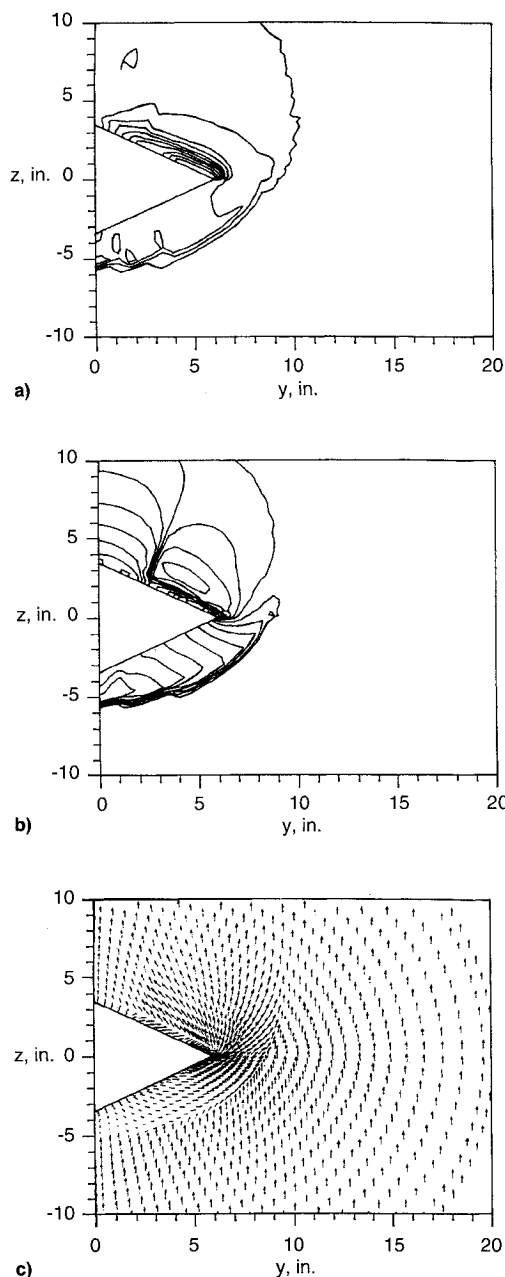

Fig. 5 Flowfield results from EMTAC at Mach 4.0, $\alpha = 15.8$ deg: a) total pressure ratio contours, b) crossflow Mach number contours, and c) crossflow velocity vectors.

range of supersonic Mach numbers. EMTAC captured the basic shape and overall levels of the surface pressure distribution over the range of supersonic Mach numbers. The good agreement between EMTAC and experiment of the force and surface pressure distribution provides a high level of confidence in the application of EMTAC for preliminary analysis of sharp-edge planforms representative of advanced military aircraft configurations.

Qualitative assessment of the computed flowfield properties and the upper-surface flow classification studies shows that EMTAC captured the flowfield characteristics associated with sharp-edged planforms. This assessment provides additional confidence for applying EMTAC in the preliminary design phase of advanced aircraft configurations. Overall, the study shows that EMTAC can be successfully applied in the preliminary analysis and design of sharp-edged advanced military aircraft.

References

[1]Szema, K., Chakravarthy, S., and Shankar, V., "Supersonic Flow Computations Using an Euler Marching Solver," NASA CR-4085, July 1987.

[2]McGrath, B. E., Covell, P. F., and Walker, I. J., "Euler Code Evaluation of a Transatmospheric Vehicle at Supersonic Speeds," AIAA Paper 89-2193, Aug. 1989.

[3]Britton, J. W., "Pressure Measurements at Supersonic Speeds on Three Uncambered Conical Wings of Unit Aspect Ratio," British Aeronautical Research Council, CP 641, 1963.

[4]Squire, L. C., "Pressure Distributions and Flow Patterns on Some Conical Shapes with Sharp Edges and Symmetrical Cross-Sections at M = 4.0," British Aeronautical Council, R.&M. No. 3340, 1963.

[5]Stanbrook, A., and Squire, L. C., "Possible Types of Flow at Swept Leading Edges," Aeronautical Quarterly, Vol. XV, Feb. 1964, pp. 72–82.

[6]Szoduch, J. G., and Peake, D. J., "Leeward Flow over Delta Wings at Supersonic Speeds," NASA TM-81187, April 1980.

[7]Miller, D. S., and Wood, R. M., "Leeside Flows over Delta Wings at Supersonic Speeds," Journal of Aircraft, Vol. 21, No. 9, 1984, pp. 680–686.

[8]Wood, R., Bauer, S., Byrd, J., McGrath, B., and Wesselmann, G., "Influence of Wing Geometry on Leading-Edge Vortices and Vortex-Induced Aerodynamics at Supersonic Speeds," AIAA Paper 89-0085, Jan. 1989.

[9]Wood, R. M., "Supersonic Aerodynamics of Delta Wings," NASA TP-2771, March 1988.

Generating Image Filters for Target Recognition by Hebbian Neural Network Learning

Alan Katz* and Philip Thrift†
Texas Instruments Incorporated, Dallas, Texas 75265

Introduction

R ECENT work[1,2] in artificial neural networks suggests mechanisms and optimization strategies that explain the

*Manager, Computational Learning Branch, Corporate R&D, P.O. Box 655936, M/S 134. Member AIAA.

†Member of Technical Staff, Corporate R&D, P.O. Box 655936, M/S 134.

formation of receptive fields, neurons sensitive to particular features, and their organization in mammalian vision systems. Not only does this work provide important clues for understanding biological vision systems, it lays the groundwork for artificial vision systems in such areas as robotics and automatic target recognition. Linsker[1] has demonstrated how Hebbian learning algorithms (GHAs), which change synaptic connections according to the degree of correlation between neuronal inputs and outputs, give rise to layers of center-surround and orientation-selective cells, even if the input to the initial layer is random white Gaussian noise.

In this Note, we apply a generalized GHA due to Sanger[3] to extract features for automatic target recognition from long-wavelength infrared (IR) and TV images. Sanger has proven that GHA determines the principal components of the data set in order of decreasing eigenvalue. Principal components or receptive fields generated with GHA are very similar in appearance to those found in Linsker's work. The novelty of our work lies in the use of GHA to generate a set of distinguishing target characteristics that separates targets from background clutter, where clutter is defined by a conventional screener algorithm to be nontarget regions in the image that have target-like characteristics.

Algorithm

We use the generalized Hebbian learning algorithm to train a one-layer neural network, where the input nodes define arrays of pixel intensity values from image data and the output nodes index the principal components. The form of the algorithm is[3]

$$c_{ij}(T + 1) = c_{ij}(T) + \gamma(T)\left[y_i(T)x_j(T) - y_i(T)\sum_{k \leq i} c_{kj}(T)y_k(T)\right] \quad (1)$$

where c_{ij} is the weight or connection strength between the jth input neuron and the ith output neuron (c_{ij} is initially assigned random weights), x_j is the jth component of the input vector, y_i is the ith component of the output vector, and $\gamma(T)$ is a learning parameter that decreases with time such that

$$\lim_{T \to \infty} \gamma(T) = 0 \quad \text{and} \quad \sum_{T=0}^{T=\infty} \gamma(T) = \infty$$

The second term on the RHS of Eq. (1) is the Hebbian term, and the third term ensures that the algorithm learns successive eigenvectors (which are the principal components), of the covariance matrix of the input vectors ordered by decreasing eigenvalue. Sanger[3] shows how Eq. (1) can be effected using only local operations, which underscores its importance for training neural networks. Other authors[4,5] have used principal components to characterize image texture.

Experiments

We apply Eq. (1) to the development of receptive fields for identifying a specific target object. To obtain inputs to the network during training, we pass a window over target subimages (no clutter region is used for training). Each position of the window defines an input vector of pixel intensities with $r \times s$ components. The network input space S, therefore, has dimension $r \times s$, and each input vector is a point in S. Network learning [Eq. (1)] produces a weight matrix c_{ij} ($1 < i < N$; $1 < j < r \times s$) that defines the top N principal components for the cluster of data points in S. A principal component corresponds to a vector in S for which the projection of data points onto the vector direction has maximum variance (which we denote as squared error), and, therefore, is maximally distinguishable. Since vectors in the input space are